IEEE Access
Multidisciplinary | Rapid Review | Open Access Journal

Received August 27, 2018, accepted September 27, 2018, date of publication October 8, 2018, date of current version October 29, 2018.

Digital Object Identifier 10.1109/ACCESS.2018.2873601

Exact and Closed-Form CRLBS for High-Order Kinematic Parameters Estimation Using LFM Coherent Pulse Train

SHUAI DING, DEFENG CHEN, HUAWEI CAO, AND TUO FU
School of Information and Electronics, Beijing Institute of Technology, Beijing 100081, China

Corresponding author: Defeng Chen (cdf2008@bit.edu.cn) and Huawei Cao (hwei.cao@gmail.com)

This work was supported in part by the National Natural Science Foundation of China under Grant 61331021 and Grant 61421001.

ABSTRACT In radar signal processing, the detection and parameter estimation of high-speed maneuvering targets, which often utilize a coherent pulse train signal with linear frequency modulation, have been receiving increasing attention. Fundamentally and significantly, the Cramer–Rao lower bound (CRLB), as a cornerstone for evaluating the estimation performance of high-order kinematic parameters, has been derived and investigated here. In this paper, a 2-D echo signal model expressed in the fast-frequency and slow-time domains is adopted. The scaled orthogonal Legendre polynomials are deliberately introduced to solve the inverse problem of the Fisher information matrix, and then, a linear mapping relationship between different polynomial parameters can be used to obtain the analytical CRLB expressions. The main contributions included are: 1) the CRLBs, which are exact and closed form, have been extended to arbitrary motion model orders and reference time instants; 2) the influences of the motion model order, the reference time instant, as well as the radar parameters on the CRLBs are exploited comprehensively; and 3) some specific cases, including four low-order motion models and two preferred reference times, are also presented to better demonstrate the CRLB performance relationships. It highlights the fact that the reference time instant corresponding to the middle of the pulse train is a reasonable and compromised choice for parameter estimation, although it is not necessarily optimal for the kinematic parameters of all models and orders. The above research results are illustrated with numerical simulations and further verified using the maximum likelihood estimation method combined with Monte Carlo experiments.

INDEX TERMS Cramer-Rao lower bound, kinematic parameter estimation, motion model order, reference time instant.

I. INTRODUCTION

The polynomial phase signal (PPS) parameter estimation problem appears in various engineering applications such as biomedicine, speech, communication, and radar signal processing and has attracted substantial research interest in the past few decades [1]. Based on the fundamental signal model with constant amplitude and polynomial phase of arbitrary degree, numerous effective estimation algorithms have been proposed and analyzed in the literature [2]–[9]. One of the most popular PPS estimators, the polynomial-phase transform (PPT) [2], also called the high-order ambiguity function (HAF) [3], accomplishes phase order decrementing via phase differentiation (PD) techniques. Subsequently, the integrated generalized ambiguity function (IGAF) [4] and the product high-order ambiguity function (PHAF) [5] can be used to suppress the cross-terms of multicomponent PPSs. In addition, time-frequency analysis [6] and time-frequency rate analysis [7] for nonstationary signals offer alternative solutions such as the polynomial Wigner-Ville distribution (PWVD) [6], [8], the high-order Wigner distribution (HO-WD) [6], [9], and the high-order cubic phase function (HO-CPF) [7], [9]. Along with the complications presented by practical application scenarios, the signal model has even been extended to the time-varying-amplitude case. It is often treated as multiplicative noise, and some cyclostationary approaches have been employed [10], [11].

To reasonably evaluate these algorithms' performance, the theoretical lower bound for unbiased estimators, well known as the Cramer-Rao Lower Bound (CRLB), provides an excellent benchmark for performance comparisons and therefore is of great importance. Peleg and Porat [12] first presented approximate but general CRLB expressions for

the constant-amplitude PPS embedded in additive white Gaussian noise. Ristic and Boashash [13] then noted in their comment that the CRLB results also depend on the observation interval over which the signal is defined. Rytel-Andrianik [14] expanded on this research and investigated the critical influence of changes in the measurement interval center on the CRLBs of PPS. Legg and Gray [15] further evaluated the bounds for polynomial phase parameter estimation with nonuniform and random sampling schemes. In addition, performance analyses of deterministic signals under both additive and multiplicative noise can be found in [16]–[18].

In the radar field, the PPS is common and usually due to a target's complex radial motion patterns. For example, when we transmit a simple sinusoidal signal, a constant-velocity motion will result in a single-tone echo signal, a constant-acceleration motion leads to a linear frequency modulation (LFM) or chirp signal, and a constant-jerk motion corresponds to a quadratic frequency modulation (QFM) signal. More generally, any continuous radial motion function on a closed time interval can be uniformly approximated by polynomials. With increasing coherent processing interval (CPI), more and more high-order motion models for maneuvering targets have been established and adopted; the relevant estimation problems of the high-order kinematic parameters are thus receiving increasing attention [19], [20]. The LFM coherent pulse train is an important waveform and is widely used in practical radar scenarios such as the long-time integration for weak target detection [21]–[23] and radar imaging for target identification [24]–[26]. For high-speed maneuvering targets, there exist envelope migration effects from pulse to pulse. Then, unlike the pure PPS case, the targets' motion information is simultaneously coupled into the envelope and phase modulations of the two-dimensional echo signal. In addition, the instantaneous kinematic parameters may be time-varying during the CPI, and it is necessary to specify a reference time instant within the pulse train for the estimation process. Correspondingly, the possible influences of designated reference times on the estimation performance are interesting and can be helpful for the envelope alignment and phase focusing operations, etc.

The maximum likelihood estimation (MLE) is one of the effective methods for the joint parameter estimation of LFM pulse train signals, and many fast implementations have been developed for low-order motion models [27]–[30]. Herein, we are concerned with the theoretical performance analysis and not a particular estimation algorithm. Abatzoglou and Gheen [27] already presented the CRLBs of range, radial velocity and acceleration using an LFM pulse train. Xu *et al.* [19] obtained the approximate CRLBs of higher order motion parameters based on the results in [12], with the reference time instant fixed at the starting pulse. Deng *et al.* [28] derived the CRLBs of some low-order motion parameters under a more accurate high-speed echo model. Pan *et al.* [31] further considered the estimation performance of a two-order motion model using a frequency modulation coded LFM pulse train. However, the last two studies did not obtain intuitive CRLB expressions. As we can see, exact and closed-form CRLBs for high-order motion models remain absent in the literature, and the influence of the reference time instant within the pulse train is rarely considered. Motivated by these facts, we will derive the analytical CRLB expressions for the high-order kinematic parameters estimation using the LFM coherent pulse train signal. Compared with current results, the performance bounds will be extended to arbitrary motion model orders and reference time instants, so they are more general and extensive.

The remainder of this paper is organized as follows. In Section 2, the echo model of an LFM coherent pulse train signal is established. The two-dimensional signal is then expressed in the fast-frequency and slow-time domains, with which the concerned estimation problem is stated. In Section 3, the scaled orthogonal Legendre polynomials are introduced to derive the Fisher information matrix. Since this matrix is close to diagonal, the exact CRLBs can be easily obtained by matrix inversion and linear mapping. In Section 4, the CRLB performance relationships are further analyzed and compared through some specific cases with different motion model orders and reference time instants. In Section 5, some numerical simulations are performed. The factor influences on the CRLBs of the kinematic parameters are illustrated, and the theoretical values are compared with the MLE results via Monte Carlo experiments. Finally, we conclude this paper and provide some future work in Section 6.

II. SIGNAL MODELING AND PROBLEM STATEMENT

A. ECHO SIGNAL MODEL

The coherent pulse train signal transmitted by a radar can be expressed as

$$\begin{aligned} s_t(t) &= \sum_m p_t(t - mT_r)\exp(j2\pi f_c t) \\ &= \sum_m p_t(\tilde{t})\exp(j2\pi f_c t) \end{aligned} \tag{1}$$

where t is the full time, $t_m = mT_r$ represents the slow-time domain, $\tilde{t} = t - t_m$ indicates the fast-time domain, T_r is the pulse repetition period, m is the pulse index, with a total pulse number of $(2M+1)$, and the dwell time is $T_D = (2M+1)T_r$. Moreover, f_c is the signal carrier frequency, and $p_t(\tilde{t})$ is the LFM waveform, with a form of

$$p_t(\tilde{t}) = \frac{1}{\sqrt{T_p}}\mathrm{rect}\left(\frac{\tilde{t}}{T_p}\right)\exp(j\pi\gamma\tilde{t}^2) \tag{2}$$

where $\mathrm{rect}(u) = \begin{cases} 1, |u| \le 1/2 \\ 0, |u| > 1/2 \end{cases}$, T_p expresses the pulse width, γ is the signal chirp rate, and the signal bandwidth B is equal to γT_p.

Without loss of generality, the observed moving target is treated as a point target, and its echo delay is denoted as τ. During the dwell time, τ is time varying with respect to the target's radial kinematic parameters. Consider that T_p is

rather small relative to T_r for a typical pulse-Doppler radar, and the effect of inter-pulse modulation is more pronounced than that of intra-pulse modulation; thus, only the inter-pulse motion is considered here. Moreover, the Doppler shift and pulse spread effects caused by a high-speed target are also ignored [28]. Then, the echo delay τ from pulse m can be further simplified as

$$\tau_m \approx \frac{2r(t_m)}{c} = \frac{2\sum_{i=0}^{I}\frac{a_i}{i!}(t_m - t_{m_0})^i}{c} \tag{3}$$

where $r(t_m)$ is the target's radial motion trajectory over a finite measurement window and c is the speed of light. Although the measurement window can be set arbitrarily like [14], for convenience, we assume that it is symmetric with $m \in \{-M, \cdots, 0, \cdots, M\}$. $t_{m_0} = m_0\, T_r$ is introduced to indicate the reference time instant within the pulse train for the high-order kinematic parameters estimation, and m_0 is used to mark the corresponding pulse index (not necessarily an integer). a_i is the relevant kinematic parameter, and the maximum motion model order is I.

According to (1)∼(3), the m-th baseband signal after pulse compression is modeled as follows

$$s_r(\tilde{t}, t_m) \approx A_r\sqrt{B}\mathrm{sinc}\left[B(\tilde{t} - \tau_m)\right] \times \exp\left[-j(2\pi f_c\tau_m + \varphi)\right] \tag{4}$$

where $\mathrm{sinc}(u) = \frac{\sin(\pi u)}{\pi u}$ and A_r and φ represent the target's scattering amplitude and initial phase, respectively. We further assume that both A_r and φ are constant during the dwell time. To facilitate the following derivations, the signal is expressed in the fast-frequency and slow-time domains [27], which gives

$$S(\tilde{f}, t_m) \approx \frac{A_r}{\sqrt{B}}\mathrm{rect}\left(\frac{\tilde{f}}{B}\right) \times \exp\left\{-j\left[\varphi + 2\pi(f_c + \tilde{f})\tau_m\right]\right\}. \tag{5}$$

In particular, if the radar bandwidth is relatively narrow and the moving target's range migration during the dwell time is not so obvious, the envelope can not provide effective constraint information, and then the above echo signal model will degenerate into a pure PPS case. Equation (5) becomes $\frac{A_r}{\sqrt{B}}\mathrm{rect}\left(\frac{\tilde{f}}{B}\right)\exp\{-j(\varphi + 2\pi f_c\tau_m)\}$.

As we know, the slow-time domain is naturally discretized with an interval of T_r, yet the fast-frequency domain is discretized as $\tilde{f} = k\Delta f$, where Δf is the frequency interval and the frequency index $k \in \{-K, \cdots, 0, \cdots, K\}$. Obviously, $B \approx (2K+1)\Delta f$. Then, the discretization signal with noise yields

$$\begin{aligned} Z(n) &= S(k,m) + W(k,m) \\ &= A\exp\left\{-j\left[\varphi + \frac{4\pi(f_c + k\Delta f)}{c}\sum_{i=0}^{I}\frac{a_i(m-m_0)^i T_r^i}{i!}\right]\right\} \\ &\quad + W(k,m) \end{aligned} \tag{6}$$

where $A = \frac{A_r}{\sqrt{B}}$ is the new amplitude defined in the frequency domain. n corresponds to the unique (k, m) pair, where $-K \le k \le K$ and $-M \le m \le M$.

The equivalent vector form of (6) is $\boldsymbol{Z} = \boldsymbol{S} + \boldsymbol{W}$, where $\boldsymbol{S}$ is the above-mentioned deterministic signal, and it can be treated as a variant of the constant-amplitude PPS. $\boldsymbol{W}$ is the additive complex Gaussian noise with zero mean and known covariance. In this situation, the total number of sampled data points is $N = (2M+1)(2K+1)$, and the parameters to be estimated are $\boldsymbol{\theta} = \{A, \varphi, a_0, a_1, \cdots, a_I\}$.

B. MAXIMUM LIKELIHOOD ESTIMATION

Based on the above echo signal model, the multidimensional joint probability density function (PDF) of $\boldsymbol{Z}$ is written as

$$\mathrm{pdf}(\boldsymbol{Z};\boldsymbol{\theta}) = \frac{1}{\pi^N \det(\boldsymbol{C_w})} \times \exp\left[-(\boldsymbol{Z}-\boldsymbol{S})^H \boldsymbol{C_w}^{-1}(\boldsymbol{Z}-\boldsymbol{S})\right] \tag{7}$$

where $\boldsymbol{C_w}$ is the covariance matrix of $\boldsymbol{W}$, "det" is the matrix determinant, and the superscript "H" means conjugate transpose. Equation (7) can also be considered as a likelihood function of $\boldsymbol{\theta}$, and hence, the corresponding log-likelihood function is

$$\begin{aligned} \Lambda(\boldsymbol{\theta};\boldsymbol{Z}) &= \ln\{\mathrm{pdf}(\boldsymbol{Z};\boldsymbol{\theta})\} \\ &\approx -(\boldsymbol{Z}-\boldsymbol{S})^H \boldsymbol{C_w}^{-1}(\boldsymbol{Z}-\boldsymbol{S}) - \ln[\det(\boldsymbol{C_w})]. \end{aligned} \tag{8}$$

The classical MLE method determines the unknown parameters by maximizing the function in (8), which means

$$\hat{\boldsymbol{\theta}} = \underset{\boldsymbol{\theta}}{\mathrm{argmax}}\ \Lambda(\boldsymbol{\theta};\boldsymbol{Z}). \tag{9}$$

It is well known that the MLE method is asymptotically effective, and evidently, its estimation performance can achieve the ideal CRLBs when the signal-to-noise ratio (SNR) is high enough. However, this method suffers from a serious computational problem because it often requires a multidimensional search over an unknown parameter space; the time consumption becomes unacceptable when the search dimension is large. Therefore, continued efforts are being made to improve the algorithm efficiency such as with the generalized Radon-Fourier transform (GRFT) [19] and the fast two-step search techniques combining the Hough transform (HT) and Newton's method [27], [28]. Moreover, researchers are also seeking suboptimal but more efficient algorithms [20], [23], [26]. Next, based on the echo signal model $\boldsymbol{Z}$ expressed in the fast-frequency and slow-time domains, as well as the given log-likelihood function $\Lambda(\boldsymbol{\theta};\boldsymbol{Z})$, we continue to derive the exact and closed-form CRLB expressions.

III. DERIVATION OF THE ANALYTICAL CRLBS

A. FISHER INFORMATION MATRIX AND ITS INVERSION

In statistical signal processing, the Fisher information provides a way of measuring the amount of information that an observable random variable carries about an unknown

parameter, and the Fisher information matrix (FIM) is generally used to calculate the covariance matrices associated with MLE. By definition, the FIM can be written as

$$\begin{aligned}\boldsymbol{J}(\boldsymbol{\theta}) &= \mathrm{E}\left\{\frac{\partial\Lambda(\boldsymbol{\theta};\boldsymbol{Z})}{\partial\boldsymbol{\theta}}\frac{\partial\Lambda(\boldsymbol{\theta};\boldsymbol{Z})}{\partial\boldsymbol{\theta}^T}\right\}\\ &= -\mathrm{E}\left\{\frac{\partial^2\Lambda(\boldsymbol{\theta};\boldsymbol{Z})}{\partial\boldsymbol{\theta}\partial\boldsymbol{\theta}^T}\right\}\end{aligned} \tag{10}$$

where "E{}" represents the mathematical expectation and the superscript "T" denotes the matrix transpose operation.

In this paper, the CRLB results under the white Gaussian noise (WGN) condition are mainly considered, and hence, $\boldsymbol{C}_{\boldsymbol{w}} = \sigma^2\boldsymbol{I}$, where σ^2 is the known noise variance and $\boldsymbol{I}$ is an identity matrix. Then, the FIM elements in (10) can be simplified as

$$\begin{aligned}\boldsymbol{J}_{\theta_i,\theta_j} &= 2\mathrm{Re}\left\{\frac{\partial\boldsymbol{S}^H}{\partial\theta_i}\boldsymbol{C}_{\boldsymbol{w}}{}^{-1}\frac{\partial\boldsymbol{S}}{\partial\theta_j}\right\}\\ &= \frac{2}{\sigma^2}\mathrm{Re}\left\{\frac{\partial\boldsymbol{S}^H}{\partial\theta_i}\frac{\partial\boldsymbol{S}}{\partial\theta_j}\right\}\end{aligned} \tag{11}$$

where "Re{}" is to obtain the real part of a complex value, and $\theta_i, \theta_j \in \boldsymbol{\theta}$. Moreover, the information matrix is symmetrical, and $\boldsymbol{J}_{\theta_i,\theta_j} = \boldsymbol{J}_{\theta_j,\theta_i}$.

For writing simplicity, we preliminarily define $\boldsymbol{S}_0 = \frac{\boldsymbol{S}}{A}$, $T_{n,i} = \frac{4\pi(f_c+k\Delta f)}{c}\frac{1}{i!}T_r^i(m-m_0)^i$, and a new matrix spanned by $T_{n,i}$ with respect to different n, which is

$$\boldsymbol{D}_i = \mathrm{diag}\left\{\left[T_{n_1,i}, T_{n_2,i}, \cdots, T_{n_N,i}\right]^T\right\} \tag{12}$$

where "diag{}" expresses a vector diagonalization operation. More intuitively, when it is specific to each estimated parameter of $\boldsymbol{\theta}$ in (11), we have

$$\boldsymbol{J}_{A,A} = \frac{2\mathrm{Re}\left\{\boldsymbol{S}_0^H\boldsymbol{S}_0\right\}}{\sigma^2} = \frac{2N}{\sigma^2} \tag{13}$$

$$\boldsymbol{J}_{\varphi,\varphi} = \frac{2\mathrm{Re}\left\{\boldsymbol{S}^H\boldsymbol{S}\right\}}{\sigma^2} = \frac{2NA^2}{\sigma^2} \tag{14}$$

$$\begin{aligned}\boldsymbol{J}_{a_{i_1},a_{i_2}} &= \frac{2\mathrm{Re}\left\{\boldsymbol{S}^H\boldsymbol{D}_{i_1}\boldsymbol{D}_{i_2}\boldsymbol{S}\right\}}{\sigma^2}\\ &= \frac{2A^2}{\sigma^2}\sum_n T_{n,i_1+i_2}^2\end{aligned} \tag{15}$$

$$\boldsymbol{J}_{A,\varphi} = \frac{2\mathrm{Re}\left\{\mathrm{j}\boldsymbol{S}_0^H\boldsymbol{S}\right\}}{\sigma^2} = 0 \tag{16}$$

$$\boldsymbol{J}_{A,a_i} = \frac{2\mathrm{Re}\left\{\mathrm{j}\boldsymbol{S}_0^H\boldsymbol{D}_i\boldsymbol{S}\right\}}{\sigma^2} = 0 \tag{17}$$

$$\boldsymbol{J}_{\varphi,a_i} = \frac{2\mathrm{Re}\left\{\boldsymbol{S}^H\boldsymbol{D}_i\boldsymbol{S}\right\}}{\sigma^2} = \frac{2A^2}{\sigma^2}\sum_n T_{n,i} \tag{18}$$

where the operation "$\sum_n$" means a two-dimensional summation "$\sum_{k=-K}^{K}\sum_{m=-M}^{M}$" here.

Thereafter, the general FIM can be summarized as (19), as shown at the top of the next page.

By inverting the information matrix in (19), the covariance matrix of the estimated parameters $\hat{\boldsymbol{\theta}}$ can be deduced. Then, the CRLB of the i-th parameter is the i-th element on the diagonal of that covariance matrix. We further obtain

$$\mathrm{var}(\hat{\theta}_i) \geq \mathrm{CRLB}(\hat{\theta}_i) = \left(\boldsymbol{J}^{-1}\right)_{i,i}. \tag{20}$$

It is not difficult to find that the estimation performance with respect to the signal amplitude is independent of that with respect to the phase parameters. As a result, the CRLB of the parameter $\hat{A}$ can simply be written as $\mathrm{var}(\hat{A}) \geq \frac{\sigma^2}{2N}$, and this parameter is no longer discussed here. However, for those polynomial phase parameters, the direct inversion of their partial FIM seems to be mathematically intractable. In this situation, although accurate CRLB results can still be obtained by numerical evaluation, the parameter dependency relationships are not so intuitive. Considering that the partial FIM is extremely ill conditioned, some authors [12], [19] have resorted to approximations. However, the derived CRLB results are tightly based on the inverse form of the Hilbert matrix, and not surprisingly, they are valid only for the starting position of the sampled signal sequence. In this research, the arbitrariness of the reference time t_{m_0} makes the matrix inversion problem more complex, and thus, we need to seek new solutions.

B. ORTHOGONAL LEGENDRE POLYNOMIALS AND THE CRLBS

To derive the exact and closed-form CRLBs, we introduce orthogonal polynomials, such as the Legendre polynomials [14], [32] or the Chebyschev polynomials [33], [34], to represent the PPS of large order. According to the properties of these polynomials, the information matrix can be reduced to an approximately diagonal form and it is much easier to find the matrix inversion. Furthermore, using the linear mapping relationship between different polynomial parameters, the required CRLBs for the high-order kinematic parameters can be obtained.

The standard, i-th Legendre polynomials $P_i(x)$ are orthogonal on $x \in [-1, 1]$. The polynomials satisfy

$$\int_{-1}^{1} P_i(x)P_j(x)dx = \begin{cases}0, & i \neq j\\ \dfrac{2}{2i+1}, & i = j\end{cases} \tag{21}$$

and $\int_{-1}^{1} P_i(x)dx$ can also be calculated through (21) when we assume $P_j(x) = P_0(x) = 1$. On this basis, we define the scaled Legendre polynomials over the interval $\left[-\frac{T_D}{2}, \frac{T_D}{2}\right]$:

$$P_i(t;T_D) = \sqrt{\frac{2}{T_D}}P_i\left(\frac{2t}{T_D}\right). \tag{22}$$

The slow-time trajectory $r(t_m)$ can be represented simultaneously with two types of polynomial forms as

$$r(t_m) = \sum_{i=0}^{I}\frac{a_i}{i!}(t_m - t_{m_0})^i = \sum_{i=0}^{I}\alpha_i P_i(t_m;T_D) \tag{23}$$

$$\boldsymbol{J}=\frac{2A^2}{\sigma^2}\begin{pmatrix}
\frac{N}{A^2} & 0 & 0 & \cdots & 0 & \cdots & 0 & \cdots & 0\\
0 & N & \sum_n T_{n,0} & \cdots & \sum_n T_{n,i_1} & \cdots & \sum_n T_{n,i_2} & \cdots & \sum_n T_{n,I}\\
0 & \sum_n T_{n,0} & \sum_n T^2_{n,0} & \cdots & \sum_n T^2_{n,i_1} & \cdots & \sum_n T^2_{n,i_2} & \cdots & \sum_n T^2_{n,I}\\
\vdots & \vdots & \vdots & \ddots & & & & & \\
0 & \sum_n T_{n,i_1} & \sum_n T^2_{n,i_1} & & \sum_n T^2_{n,2i_1} & & \sum_n T^2_{n,i_1+i_2} & & \sum_n T^2_{n,i_1+I}\\
\vdots & \vdots & \vdots & & & \ddots & & & \\
0 & \sum_n T_{n,i_2} & \sum_n T^2_{n,i_2} & & \sum_n T^2_{n,i_1+i_2} & & \sum_n T^2_{n,2i_2} & & \sum_n T^2_{n,i_2+I}\\
\vdots & \vdots & \vdots & & & & & \ddots & \\
0 & \sum_n T_{n,I} & \sum_n T^2_{n,I} & & \sum_n T^2_{n,i_1+I} & & \sum_n T^2_{n,i_2+I} & & \sum_n T^2_{n,2I}
\end{pmatrix}. \tag{19}$$

$$\boldsymbol{J'}=\frac{2A^2}{\sigma^2}\begin{pmatrix}
N & \frac{\beta_1}{T_r}\sqrt{2T_D} & \cdots & 0 & \cdots & 0 & \cdots & 0\\
\frac{\beta_1}{T_r}\sqrt{2T_D} & \frac{\beta_2}{T_r}2 & \cdots & 0 & \cdots & 0 & \cdots & 0\\
\vdots & \vdots & \ddots & & & & & \\
0 & 0 & & \frac{\beta_2}{T_r}\frac{2}{2i_1+1} & & 0 & & 0\\
\vdots & \vdots & & & \ddots & & & \\
0 & 0 & & 0 & & \frac{\beta_2}{T_r}\frac{2}{2i_2+1} & & 0\\
\vdots & \vdots & & & & & \ddots & \\
0 & 0 & & 0 & & 0 & & \frac{\beta_2}{T_r}\frac{2}{2I+1}
\end{pmatrix} \tag{24}$$

where $\alpha_{i,0\le i\le I}$ are the relevant coefficients of the new scaled Legendre polynomials. Note that the discrete Legendre polynomials in (23) can maintain their orthogonality with respect to t_m if the number of sampling points in the slow-time domain is sufficiently large. Then, we can repeat the previous calculation steps, and a reconstructed information matrix $\boldsymbol{J'}$ for the phase parameters $\boldsymbol{\theta'}=\{\varphi,\alpha_0,\cdots,\alpha_I\}$ is written as (24), as shown at the top of this page, where the auxiliary factors β_1 and β_2 are defined as follows:

$$\beta_1=\sum_{k=-K}^{K}\frac{4\pi(f_c+k\Delta f)}{c}=\frac{4\pi f_c}{c}(2K+1) \tag{25}$$

and

$$\begin{aligned}\beta_2&=\sum_{k=-K}^{K}\left[\frac{4\pi(f_c+k\Delta f)}{c}\right]^2\\&=\frac{16\pi^2(2K+1)}{c^2}\left[f_c^2+\frac{K(K+1)}{3}\Delta f^2\right].\end{aligned} \tag{26}$$

Inverting the near-diagonal information matrix in (24), we can subsequently obtain

$$\begin{aligned}\mathrm{var}(\hat{\varphi})&\ge\frac{\sigma^2}{2A^2}\frac{\beta_2}{(2M+1)\left[(2K+1)\beta_2-\beta_1^2\right]}\\&=\frac{\sigma^2}{2NA^2}\frac{f_c^2+K(K+1)\Delta f^2/3}{K(K+1)\Delta f^2/3}\end{aligned} \tag{27}$$

and

$$\begin{aligned}\mathrm{var}(\hat{\alpha_0})&\ge\frac{\sigma^2}{4A^2}\frac{(2K+1)T_r}{\left[(2K+1)\beta_2-\beta_1^2\right]}\\&=\frac{\sigma^2}{2NA^2}\frac{T_D}{32\pi^2}\frac{c^2}{K(K+1)\Delta f^2/3}\end{aligned} \tag{28}$$

$$\begin{aligned}\mathrm{var}(\hat{\alpha_i})&\ge\frac{\sigma^2}{4A^2}\frac{T_r}{\beta_2}=\frac{\sigma^2}{2NA^2}\frac{T_D}{32\pi^2}(2i+1)\\&\quad\times\frac{c^2}{f_c^2+K(K+1)\Delta f^2/3},\quad 1\le i\le I.\end{aligned} \tag{29}$$

Notice that the estimation performance of the initial phase $\hat{\varphi}$ is coupled with that of the range-related parameter $\hat{\alpha}_0$. Despite having the same order 0, their identifiability is based

on the fact that $\hat{\varphi}$ is determined only by the phase information, but $\hat{\alpha}_0$ is constrained by both the envelope information and the phase information. For $1 \le i \le I$, the estimation performance of the parameter $\hat{\alpha}_i$ is independent of each other, and its CRLB is a linear function of the order i.

According to (23), there exists a linear mapping relationship between the two types of polynomial coefficients:

$$\boldsymbol{a} = \boldsymbol{P} \cdot \boldsymbol{\alpha} \tag{30}$$

where $\boldsymbol{a} = \{a_0, a_1, \cdots, a_I\}^T$ and $\boldsymbol{\alpha} = \{\alpha_0, \alpha_1, \cdots, \alpha_I\}^T$. $\boldsymbol{P}$ is an upper triangular matrix with the element p_{ij} $(j \ge i)$ in row i and column j.

The standard Legendre polynomials can also be expanded as $P_j(x) = \sum_{l=0}^{\lfloor j/2 \rfloor} (-1)^l \frac{(2j-2l)!}{2^j l!(j-l)!(j-2l)!} x^{j-2l}$, where "$\lfloor\rfloor$" denotes the integer floor function. Substituting it into the above formulas, we can obtain the specific expression of p_{ij}. It shows that

$$p_{ij} = \sqrt{\frac{2}{T_D}} \frac{1}{T_D^i} \sum_{l=0}^{\lfloor (j-i)/2 \rfloor} \frac{(-1)^l}{2^{2l}} \times \frac{(2j-2l)!}{l!(j-l)!(j-i-2l)!} \left(\frac{t_{m_0}}{T_D}\right)^{j-i-2l}. \tag{31}$$

Consequently, the estimation covariance of $\hat{\boldsymbol{a}}$ can be transformed from that of $\hat{\boldsymbol{\alpha}}$ with the above affine matrix $\boldsymbol{P}$, which means

$$\boldsymbol{C}_{\hat{\boldsymbol{a}}} = \boldsymbol{P} \cdot \boldsymbol{C}_{\hat{\boldsymbol{\alpha}}} \cdot \boldsymbol{P}^T. \tag{32}$$

Finally, with (28)$\sim$(32), the exact and closed-form CRLBs for estimating the high-order kinematic parameters $(1 \le i \le I)$ are expressed as

$$\begin{aligned} &\mathrm{CRLB}(\hat{a}_i) \\ &= \sum_{j=i}^{I} p_{ij}^2 \cdot \mathrm{CRLB}(\hat{\alpha}_j) \\ &= \frac{\lambda_a^2}{32\pi^2 \mathrm{SNR}_N T_D^{2i}} \sum_{j=i}^{I} (2j+1) \\ &\quad \times \left[\sum_{l=0}^{\lfloor (j-i)/2 \rfloor} \frac{(-1)^l}{2^{2l}} \frac{(2j-2l)!}{l!(j-l)!(j-i-2l)!} \eta^{j-i-2l} \right]^2 \end{aligned} \tag{33}$$

where $\mathrm{SNR}_N = \frac{NA^2}{\sigma^2}$ is the accumulated SNR, $\eta = \frac{t_{m_0}}{T_D} = \frac{m_0}{2M+1}$ is a normalization reference time factor of the reference time instant t_{m_0} relative to the accumulated time T_D, and $\lambda_a = \frac{c}{\sqrt{f_c^2 + K(K+1)\Delta f^2/3}}$ is defined as an equivalent wavelength, constituted by the actual signal wavelength $\lambda_c = \frac{c}{f_c}$, as well as its root mean square (RMS) wavelength $\lambda_b = \frac{c}{\sqrt{K(K+1)\Delta f^2/3}}$. Herein, we have $\frac{1}{\lambda_a^2} = \frac{1}{\lambda_b^2} + \frac{1}{\lambda_c^2}$ and $\lambda_b \approx \frac{c}{B/\sqrt{12}}$. The above CRLBs are related to both the signal frequency f_c and the signal bandwidth B. Similarly, the CRLBs for the pure PPS case can also be derived, and the multiplicative factor λ_a in (33) will be replaced by λ_c which is only connected with the signal frequency f_c.

For the special case of the range parameter $\hat{a}_0$, because the CRLB of $\hat{\alpha}_0$ in (28) does not conform to the general form of $\hat{\alpha}_i$ in (29), we need to make some minor corrections in (33). Specifically,

$$\mathrm{CRLB}'(\hat{a}_0) = \mathrm{CRLB}(\hat{a}_0) + \frac{\lambda_b^2 - \lambda_a^2}{32\pi^2 \mathrm{SNR}_N} \tag{34}$$

where the additional quantity is denoted $\Delta_{\hat{a}_0}$ here. Since $\Delta_{\hat{a}_0} > 0$, the actual estimation performance of $\hat{a}_0$ degrades due to the negative influence of the unknown initial phase φ. For a typical narrowband radar, $B \ll f_c$, $\lambda_b \gg \lambda_a$, and thus, $\Delta_{\hat{a}_0}$ plays a major role in (34). Moreover, $\Delta_{\hat{a}_0}$ also decreases with increasing SNR_N. While for the pure PPS, the range parameter a_0 can not be distinguished from the initial phase parameter φ by the phase information.

In general, (33) and (34) provide more extensive performance bounds for the high-order kinematic parameters estimation. All the relevant factors have clear physical meanings, and their relationships with the CRLBs can be studied analytically and quantitatively. Preliminarily, the derived analytical expressions reveal some useful properties of the CRLBs:

- The CRLBs of high-order kinematic parameters are independent of the parameter values themselves.
- The large model order I normally increases the CRLBs of the kinematic parameters, which implies that the estimation performance is degraded. This is easy to understand because the number of unknown parameters to be estimated increases.
- Except for the highest order parameter $\hat{a}_I$, the CRLBs of other order kinematic parameters $\hat{a}_i$ are always $2(I-i)$-order polynomial functions of the reference time factor η, and these functions are also even symmetrical.
- The CRLBs are inversely proportional to the accumulated SNR, and the i-th parameter is inversely proportional to the $2i$ power of the accumulated time T_D.
- The CRLBs are also related to the signal frequency f_c and its bandwidth B, and increasing them helps to achieve better estimation performance.

In the following section, we will further analyze the CRLB performance relationships through some more specific cases. The CRLB results with respect to different motion model orders and reference time instants are demonstrated and compared.

IV. CRLB ANALYSIS AND COMPARISONS THROUGH SOME SPECIFIC CASES

A. WITH DIFFERENT MOTION MODEL ORDERS

Considering the radar observation scenarios most frequently encountered in practical applications, we mainly present here the analytical CRLB expressions of different order kinematic parameters with $I = 1, 2, 3, 4$.

$I = 1$ corresponds to a constant-velocity motion scenario. Then, the CRLBs of the radial range $\hat{a}_{1,0}$ and velocity $\hat{a}_{1,1}$ are simplified as

$$\begin{cases} \mathrm{CRLB}'\left(\hat{a}_{1,0}\right) = \dfrac{\lambda_a^2}{32\pi^2 \mathrm{SNR}_N}(1+12\eta^2) + \Delta_{\hat{a}_0} \\ \mathrm{CRLB}\left(\hat{a}_{1,1}\right) = \dfrac{3\lambda_a^2}{8\pi^2 \mathrm{SNR}_N T_D^2} \end{cases} \tag{35}$$

Obviously, only the CRLB of $\hat{a}_{1,0}$ is related to the reference time factor η, and it obtains the minimum CRLB value at $\eta = 0$. For convenience, the optimal reference time factor is denoted η_{opt} here.

$I = 2$ corresponds to a constant-acceleration motion scenario. The CRLBs of the radial range $\hat{a}_{2,0}$, velocity $\hat{a}_{2,1}$, and acceleration $\hat{a}_{2,2}$ are

$$\begin{cases} \mathrm{CRLB}'\left(\hat{a}_{2,0}\right) = \dfrac{9\lambda_a^2}{128\pi^2 \mathrm{SNR}_N}(1-8\eta^2+80\eta^4) + \Delta_{\hat{a}_0} \\ \mathrm{CRLB}\left(\hat{a}_{2,1}\right) = \dfrac{3\lambda_a^2}{8\pi^2 \mathrm{SNR}_N T_D^2}(1+60\eta^2) \\ \mathrm{CRLB}\left(\hat{a}_{2,2}\right) = \dfrac{45\lambda_a^2}{2\pi^2 \mathrm{SNR}_N T_D^4} \end{cases} \tag{36}$$

Now, the CRLBs of $\hat{a}_{2,0}$ and $\hat{a}_{2,1}$ are related to η, and the optimal reference time factors for the radial range and velocity estimation are $\eta_{\mathrm{opt}} = \pm\frac{1}{2\sqrt{5}}, 0$. It is not difficult to find that the CRLBs derived in [27] are special cases of the above formulas when $\eta = 0$.

$I = 3$ represents what has recently become a relatively popular constant-jerk motion model. The CRLBs of the radial range $\hat{a}_{3,0}$, velocity $\hat{a}_{3,1}$, acceleration $\hat{a}_{3,2}$, and jerk $\hat{a}_{3,3}$ are written as

$$\begin{cases} \mathrm{CRLB}'\left(\hat{a}_{3,0}\right) = \dfrac{9\lambda_a^2}{128\pi^2 \mathrm{SNR}_N} \\ \qquad \times (1+20\eta^2 - \dfrac{880}{3}\eta^4 + \dfrac{11200}{9}\eta^6) + \Delta_{\hat{a}_0} \\ \mathrm{CRLB}\left(\hat{a}_{3,1}\right) = \dfrac{75\lambda_a^2}{32\pi^2 \mathrm{SNR}_N T_D^2}(1-24\eta^2+336\eta^4) \\ \mathrm{CRLB}\left(\hat{a}_{3,2}\right) = \dfrac{45\lambda_a^2}{2\pi^2 \mathrm{SNR}_N T_D^4}(1+140\eta^2) \\ \mathrm{CRLB}\left(\hat{a}_{3,3}\right) = \dfrac{3150\lambda_a^2}{\pi^2 \mathrm{SNR}_N T_D^6} \end{cases} \tag{37}$$

Under this model, the optimal reference time factors for estimating the radial range, velocity, and acceleration become $\eta_{\mathrm{opt}} = 0, \pm\frac{1}{2\sqrt{7}}$, and 0.

$I = 4$ represents a more dynamic maneuvering model. Correspondingly, the CRLBs of the radial range $\hat{a}_{4,0}$, velocity $\hat{a}_{4,1}$, acceleration $\hat{a}_{4,2}$, jerk $\hat{a}_{4,3}$, and snap $\hat{a}_{4,4}$ are

$$\begin{cases} \mathrm{CRLB}'\left(\hat{a}_{4,0}\right) = \dfrac{225\lambda_a^2}{2048\pi^2 \mathrm{SNR}_N}(1-16\eta^2+\dfrac{1568}{3}\eta^4 \\ \qquad - \dfrac{41216}{9}\eta^6 + 12544\eta^8) + \Delta_{\hat{a}_0} \\ \mathrm{CRLB}\left(\hat{a}_{4,1}\right) = \dfrac{75\lambda_a^2}{32\pi^2 \mathrm{SNR}_N T_D^2} \\ \qquad \times (1+84\eta^2 - 1680\eta^4 + 9408\eta^6) \\ \mathrm{CRLB}\left(\hat{a}_{4,2}\right) = \dfrac{2205\lambda_a^2}{8\pi^2 \mathrm{SNR}_N T_D^4}(1-40\eta^2+720\eta^4) \\ \mathrm{CRLB}\left(\hat{a}_{4,3}\right) = \dfrac{3150\lambda_a^2}{\pi^2 \mathrm{SNR}_N T_D^6}(1+252\eta^2) \\ \mathrm{CRLB}\left(\hat{a}_{4,4}\right) = \dfrac{793800\lambda_a^2}{\pi^2 \mathrm{SNR}_N T_D^8} \end{cases} \tag{38}$$

Similarly, we can also find that the CRLBs of $\hat{a}_{4,0}$, $\hat{a}_{4,1}$, $\hat{a}_{4,2}$, and $\hat{a}_{4,3}$ in (38) obtain their respective minimum values at $\eta_{\mathrm{opt}} = \pm\frac{1}{2}\sqrt{\frac{7-2\sqrt{7}}{21}}, 0, \pm\frac{1}{6}$, and 0.

According to the above analysis, it can be observed that the optimal reference time instants are remarkably inconsistent for different order kinematic parameters even at the same motion model. Especially, as for the parameter $a_{I,i}(i \neq I)$, if the order $(I-i)$ is odd, η_{opt} is always 0; if the order $(I-i)$ is even, η_{opt} approaches the vicinity of 0 with the increase in I.

B. WITH DIFFERENT REFERENCE TIME INSTANTS

In practice, the starting and middle pulse positions are the two most preferred reference time instants to align the pulse train envelope and to estimate the relevant kinematic parameters. For the starting pulse case, we know that $m_0 = -M$, and the reference time factor $\eta = -\frac{M}{2M+1}$. It approximates to $-\frac{1}{2}$ if $M \gg 1$; for the middle pulse case, we know that $m_0 = 0$, and the reference time factor $\eta = 0$. Then, with the results in [14], the simplified CRLB expressions at $\eta = -\frac{1}{2}$ and $\eta = 0$ can be easily written.

Substituting $\eta = -\frac{1}{2}$ into (33), we can obtain

$$\mathrm{CRLB}(\hat{a}_i) = \frac{\lambda_a^2}{32\pi^2 \mathrm{SNR}_N T_D^{2i}} \frac{(i!)^2}{2i+1} \times \left[(I+i+1)\binom{I+i}{i}\binom{I}{i}\right]^2 \tag{39}$$

where the combination number $\binom{n}{m} = \frac{n!}{m!(n-m)!}$.

On the one hand, (39) is quite similar in form to the frequently cited CRLB results in [12], but the derived analytical expressions are exact, making it superior. On the other hand, as preliminarily discussed in [19], it is noted that the performance differences between the LFM coherent pulse train signal and the pure PPS are mainly reflected in their multiplicative coefficients (related to λ_a^2 and λ_c^2, respectively, here). It is

TABLE 1. CRLB comparisons of the high-order kinematic parameters.

Kinematic parameters	$\eta=-\frac{1}{2}$	$\eta=0$	η_{opt}
$\hat{a}_{1,0}$	$\frac{\lambda_a^2}{8\pi^2\text{SNR}_N}+\Delta_{\hat{a}_0}$	$\frac{\lambda_a^2}{32\pi^2\text{SNR}_N}+\Delta_{\hat{a}_0}$	$\frac{\lambda_a^2}{32\pi^2\text{SNR}_N}+\Delta_{\hat{a}_0}$
$\hat{a}_{1,1}$	$\frac{3\lambda_a^2}{8\pi^2\text{SNR}_N T_D^2}$	$\frac{3\lambda_a^2}{8\pi^2\text{SNR}_N T_D^2}$	$\frac{3\lambda_a^2}{8\pi^2\text{SNR}_N T_D^2}$
$\hat{a}_{2,0}$	$\frac{9\lambda_a^2}{32\pi^2\text{SNR}_N}+\Delta_{\hat{a}_0}$	$\frac{9\lambda_a^2}{128\pi^2\text{SNR}_N}+\Delta_{\hat{a}_0}$	$\frac{9\lambda_a^2}{160\pi^2\text{SNR}_N}+\Delta_{\hat{a}_0}$
$\hat{a}_{2,1}$	$\frac{6\lambda_a^2}{\pi^2\text{SNR}_N T_D^2}$	$\frac{3\lambda_a^2}{8\pi^2\text{SNR}_N T_D^2}$	$\frac{3\lambda_a^2}{8\pi^2\text{SNR}_N T_D^2}$
$\hat{a}_{2,2}$	$\frac{45\lambda_a^2}{2\pi^2\text{SNR}_N T_D^4}$	$\frac{45\lambda_a^2}{2\pi^2\text{SNR}_N T_D^4}$	$\frac{45\lambda_a^2}{2\pi^2\text{SNR}_N T_D^4}$
$\hat{a}_{3,0}$	$\frac{\lambda_a^2}{2\pi^2\text{SNR}_N}+\Delta_{\hat{a}_0}$	$\frac{9\lambda_a^2}{128\pi^2\text{SNR}_N}+\Delta_{\hat{a}_0}$	$\frac{9\lambda_a^2}{128\pi^2\text{SNR}_N}+\Delta_{\hat{a}_0}$
$\hat{a}_{3,1}$	$\frac{75\lambda_a^2}{2\pi^2\text{SNR}_N T_D^2}$	$\frac{75\lambda_a^2}{32\pi^2\text{SNR}_N T_D^2}$	$\frac{75\lambda_a^2}{56\pi^2\text{SNR}_N T_D^2}$
$\hat{a}_{3,2}$	$\frac{810\lambda_a^2}{\pi^2\text{SNR}_N T_D^4}$	$\frac{45\lambda_a^2}{2\pi^2\text{SNR}_N T_D^4}$	$\frac{45\lambda_a^2}{2\pi^2\text{SNR}_N T_D^4}$
$\hat{a}_{3,3}$	$\frac{3150\lambda_a^2}{\pi^2\text{SNR}_N T_D^6}$	$\frac{3150\lambda_a^2}{\pi^2\text{SNR}_N T_D^6}$	$\frac{3150\lambda_a^2}{\pi^2\text{SNR}_N T_D^6}$
$\hat{a}_{4,0}$	$\frac{25\lambda_a^2}{32\pi^2\text{SNR}_N}+\Delta_{\hat{a}_0}$	$\frac{225\lambda_a^2}{2048\pi^2\text{SNR}_N}+\Delta_{\hat{a}_0}$	$\frac{25(14-\sqrt{7})\lambda_a^2}{3024\pi^2\text{SNR}_N}+\Delta_{\hat{a}_0}$
$\hat{a}_{4,1}$	$\frac{150\lambda_a^2}{\pi^2\text{SNR}_N T_D^2}$	$\frac{75\lambda_a^2}{32\pi^2\text{SNR}_N T_D^2}$	$\frac{75\lambda_a^2}{32\pi^2\text{SNR}_N T_D^2}$
$\hat{a}_{4,2}$	$\frac{19845\lambda_a^2}{2\pi^2\text{SNR}_N T_D^4}$	$\frac{2205\lambda_a^2}{8\pi^2\text{SNR}_N T_D^4}$	$\frac{245\lambda_a^2}{2\pi^2\text{SNR}_N T_D^4}$
$\hat{a}_{4,3}$	$\frac{201600\lambda_a^2}{\pi^2\text{SNR}_N T_D^6}$	$\frac{3150\lambda_a^2}{\pi^2\text{SNR}_N T_D^6}$	$\frac{3150\lambda_a^2}{\pi^2\text{SNR}_N T_D^6}$
$\hat{a}_{4,4}$	$\frac{793800\lambda_a^2}{\pi^2\text{SNR}_N T_D^8}$	$\frac{793800\lambda_a^2}{\pi^2\text{SNR}_N T_D^8}$	$\frac{793800\lambda_a^2}{\pi^2\text{SNR}_N T_D^8}$

known that $\lambda_a^2=\lambda_c^2\left(1-\frac{\lambda_c^2}{\lambda_b^2+\lambda_c^2}\right)$, and thus, $\lambda_a^2<\lambda_c^2$. This means that the estimation performance based on the LFM coherent pulse train signal is better since it introduces extra envelope constraints into the phase information. Furthermore, the large signal bandwidth also facilities better estimation results. As expected, a larger bandwidth B implies a higher range resolution $\frac{c}{2B}$ such that the target's migration effect is more obvious, and then, the envelope information provides more benefits to the parameter estimation. The above analysis can be easily generalized to other η as well.

Substituting $\eta=0$ into (33), we also have

$$\text{CRLB}(\hat{a}_i)=\frac{\lambda_a^2}{32\pi^2\text{SNR}_N T_D^{2i}}\frac{(i!)^2}{2i+1}\times\left[\frac{2s+2i+1}{2^{2s}}\binom{2s+2i}{i}\binom{2s+i}{s}\right]^2 \quad (40)$$

where $s=\lfloor\frac{I-i}{2}\rfloor$.

Unlike the former case, the CRLBs in (40) are associated with the motion model order I through an indirect relationship $\lfloor\frac{I-i}{2}\rfloor$. This indicates that the estimation performance of the same parameter $\hat{a}_i$ remains unchanged when the order $(I-i)$ increases from even to odd. Moreover, with (39) and (40), it can be observed that the CRLB results obtained at $\eta=0$ are relatively close to optimality, which are generally much smaller than those obtained at $\eta=-\frac{1}{2}$. For example, under a constant-jerk motion model ($I=3$), the CRLB of the radial velocity $\hat{a}_{3,1}$ with respect to $\eta=-\frac{1}{2}$ is 16 times that with respect to $\eta=0$.In contrast, the latter is only 1.75 times that with respect to η_{opt}. More detailed CRLB comparisons with respect to different motion model orders and reference time factors are summarized in Tab. 1. Combined with the previous discussions, it is recommended to use the reference time instant corresponding to the middle of the pulse train ($\eta=0$) for the parameter estimation, although it is not necessarily optimal for the kinematic parameters of all models and orders.

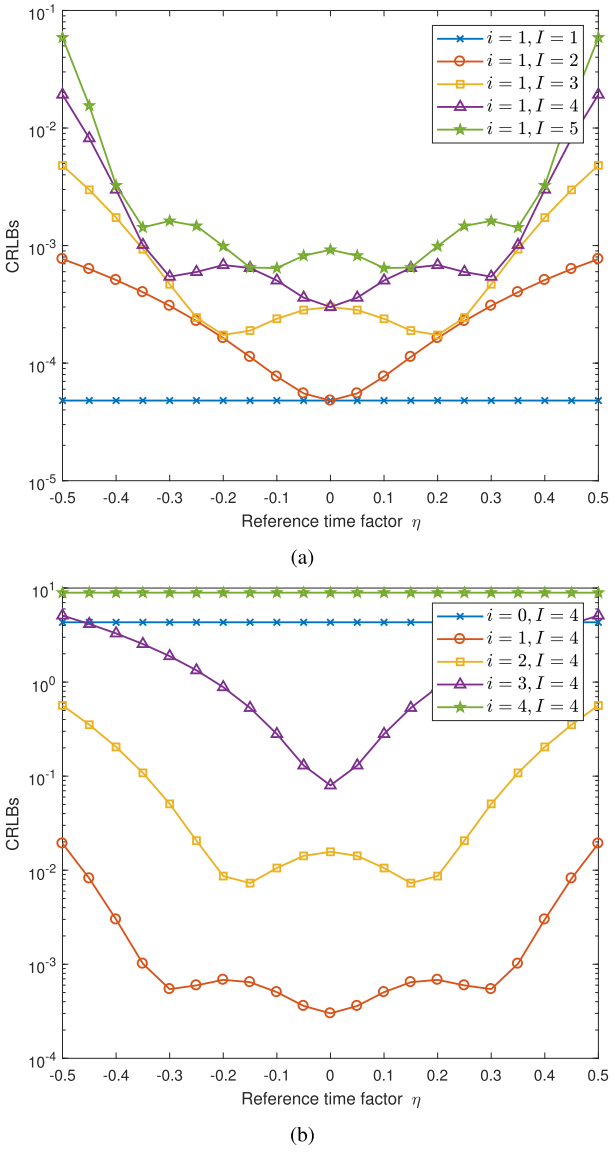

FIGURE 1. CRLBs vs reference time factor. (a) velocity estimation performance under different motion models ($I=1\sim5$). (b) CRLBs of different order kinematic parameters under the same motion model ($I=4$).

With regard to potential applications, the above CRLB results can provide a quantitative aid in determining the radar operating parameters, such as the signal frequency, the signal bandwidth and the accumulated time. As a performance benchmark, the analytical CRLBs can also be used to define the asymptotic relative efficiency (ARE) for evaluating the estimation performance of various algorithms [3]. And a smaller ARE denotes a better parameter estimation performance. At high SNR, if ARE is equal to 1, then the estimation performance achieves the CRLB, which means that the estimation method is asymptotically effective, just like the MLE method.

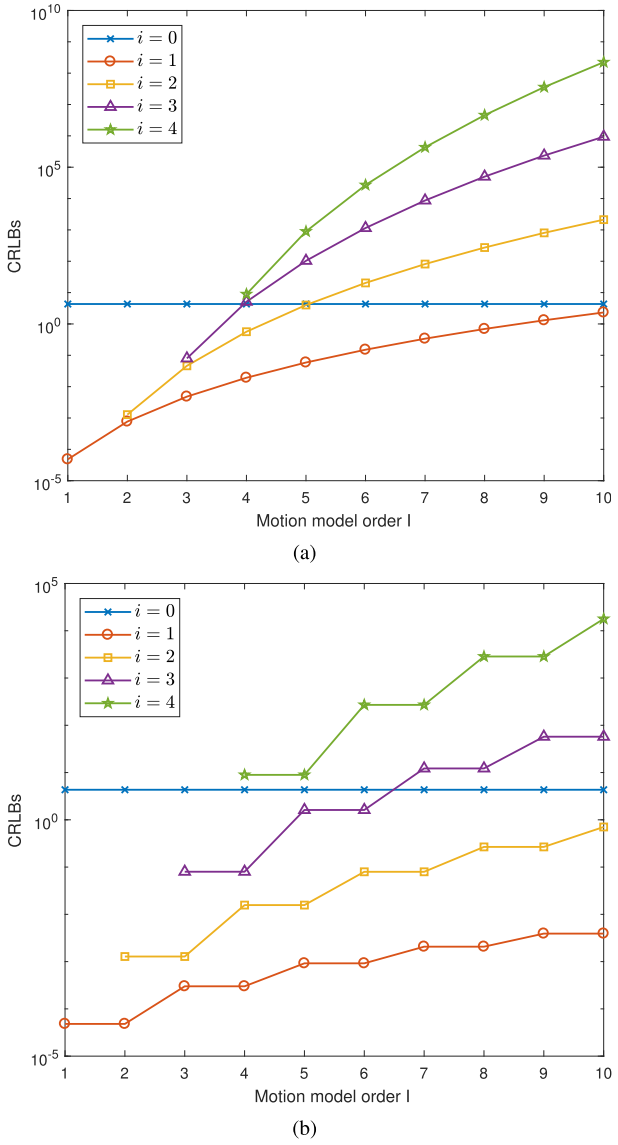

FIGURE 2. CRLBs vs motion model order. (a) reference time factor $\eta = -\frac{1}{2}$. (b) reference time factor $\eta = 0$.

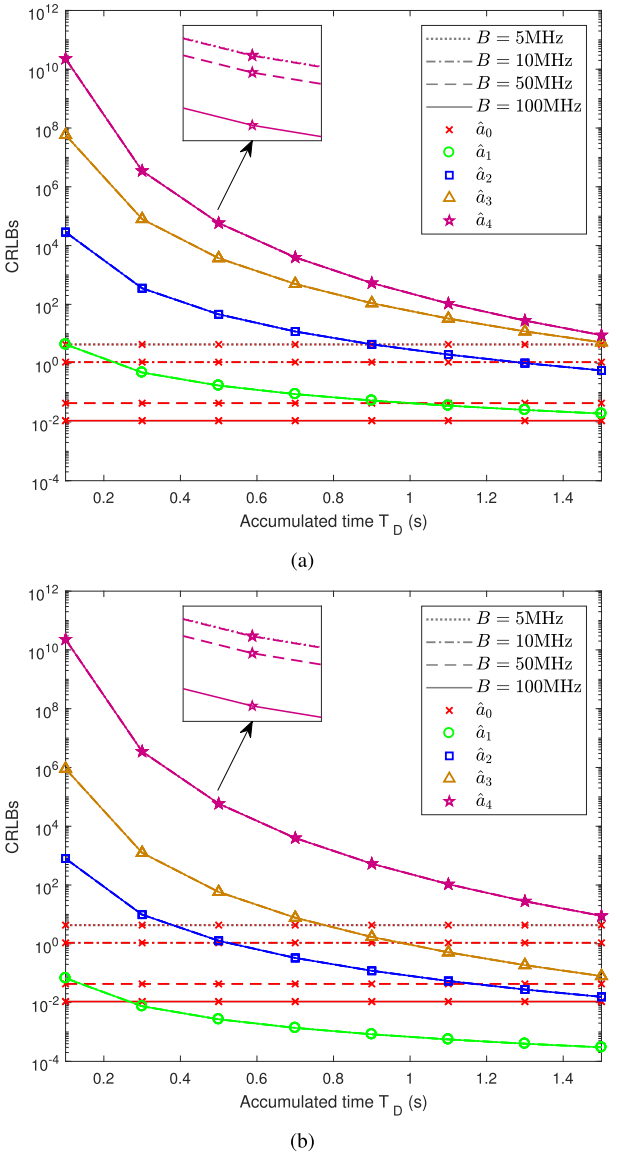

FIGURE 3. CRLBs vs accumulated time and signal bandwidth. (a) reference time factor $\eta = -\frac{1}{2}$. (b) reference time factor $\eta = 0$.

In addition, the estimation performance of the highest order kinematic parameter $\hat{a}_I$ is constant and independent of the reference time factor η, and thus, its CRLB can be written as $\frac{\lambda_a^2(2I+1)}{32\pi^2 \mathrm{SNR}_N T_D^{2I}} \binom{2I}{I}^2$. In practical processing, the maximum order I may be unknown as well. Through the parameter estimation and comparisons with this theoretical result, a reasonable motion model order can be determined similar to [2].

V. NUMERICAL SIMULATIONS

In this section, we further verify the above theoretical results with some numerical simulations. The influences of relevant factors on the CRLBs for estimating the high-order kinematic parameters are illustrated and discussed. Then, the derived CRLBs under four motion models are also confirmed by comparing with the Monte Carlo experiment results of the MLE method.

First, we will illustrate the main influences of the reference time factor η on the parameter estimation performance. Two specific situations are highlighted here: the same parameter estimation results under different order motion models and the estimation results of different parameters under the same motion model. In this simulation, we suppose that the signal carrier frequency $f_c = 1$ GHz, its bandwidth $B = 5$ MHz, the accumulated time is 1.5 s, and the accumulated SNR is 15 dB. η ranges from $-\frac{1}{2}$ to $\frac{1}{2}$. Fig. 1 (a) presents the CRLBs of the radial velocity ($i = 1$) versus η when the model order I is equal to 1, 2, 3, 4 and 5. Fig. 1 (b) shows the respective CRLBs of the radial range, velocity, acceleration, jerk and snap versus η when the model order $I = 4$. The simulation

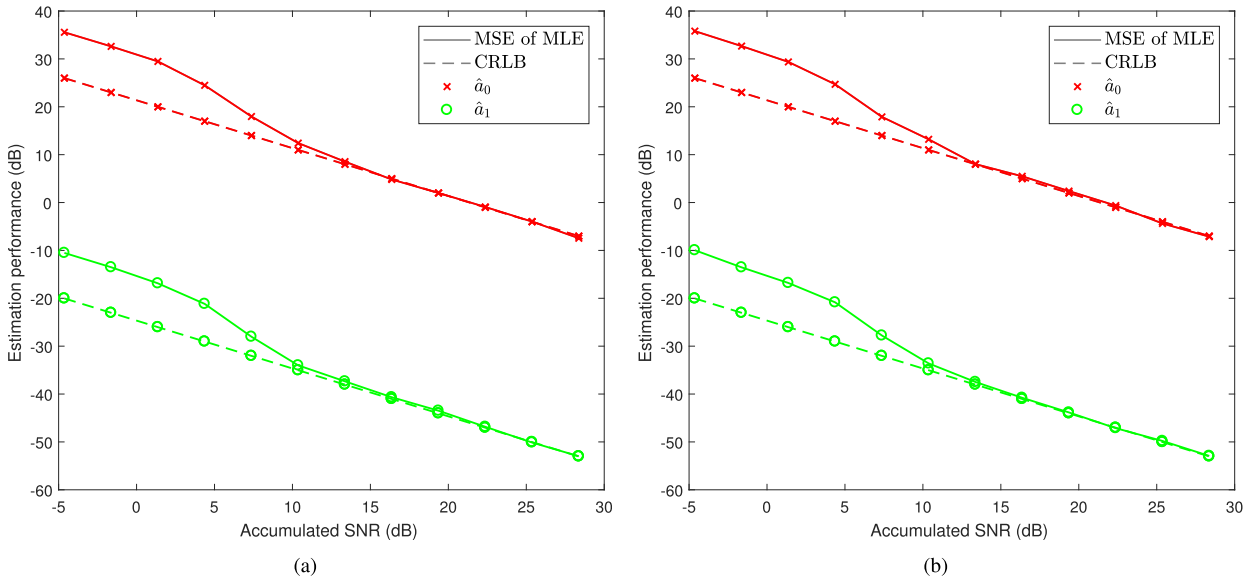

FIGURE 4. Comparisons of the MLE estimation performance and the CRLBs under a first-order motion model. (a) reference time factor $\eta = -\frac{1}{2}$. (b) reference time factor $\eta = 0$.

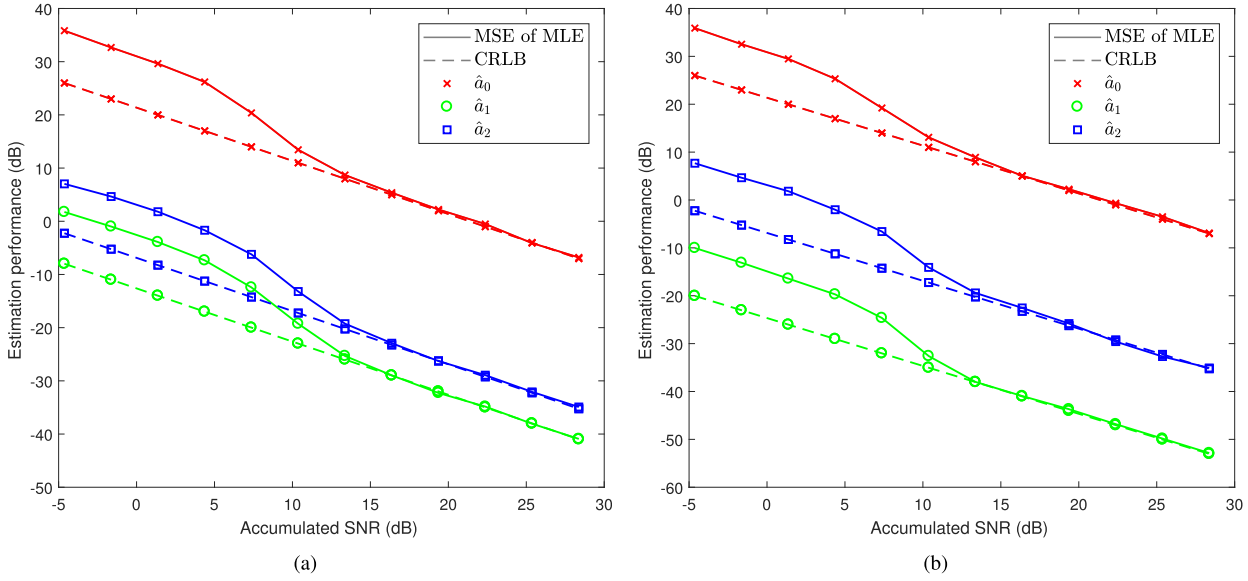

FIGURE 5. Comparisons of the MLE estimation performance and the CRLBs under a second-order motion model. (a) reference time factor $\eta = -\frac{1}{2}$. (b) reference time factor $\eta = 0$.

results clearly reveal the existing inconsistency of the optimal η for the parameter estimation with respect to different i and I. And the CRLBs at $\eta = 0$ are relatively close to those at η_{opt}, usually no more than twice. Comprehensively, $\eta = 0$ is a more reasonable and suitable choice for the LFM pulse train signal processing.

Second, we also exploit the influences of the order i and I on the parameter estimation performance. Two representative reference time instants, the starting pulse case ($\eta = -\frac{1}{2}$) and the middle pulse case ($\eta = 0$), are mainly considered and compared here. Similarly, the signal frequency is set to 1 GHz, the signal bandwidth is 5 MHz, the accumulated time is 1.5 s, and the accumulated SNR is 15 dB. The parameter order i varies from 0 to 4, and the model order I ranges from 1 to 10 with a step size of 1. Fig. 2 (a) and (b) present the CRLBs of the parameter $\hat{a}_i$ versus I at $\eta = -\frac{1}{2}$ and $\eta = 0$, respectively. It can be observed that, for the same i, the CRLB values of $\hat{a}_i$ generally increase with the motion order I. In particular, there is a value jump phenomenon (stage change) in the case of $\eta = 0$, which agrees with the results obtained from (38). In most situations, the estimation performance of the high-order kinematic parameters at $\eta = 0$

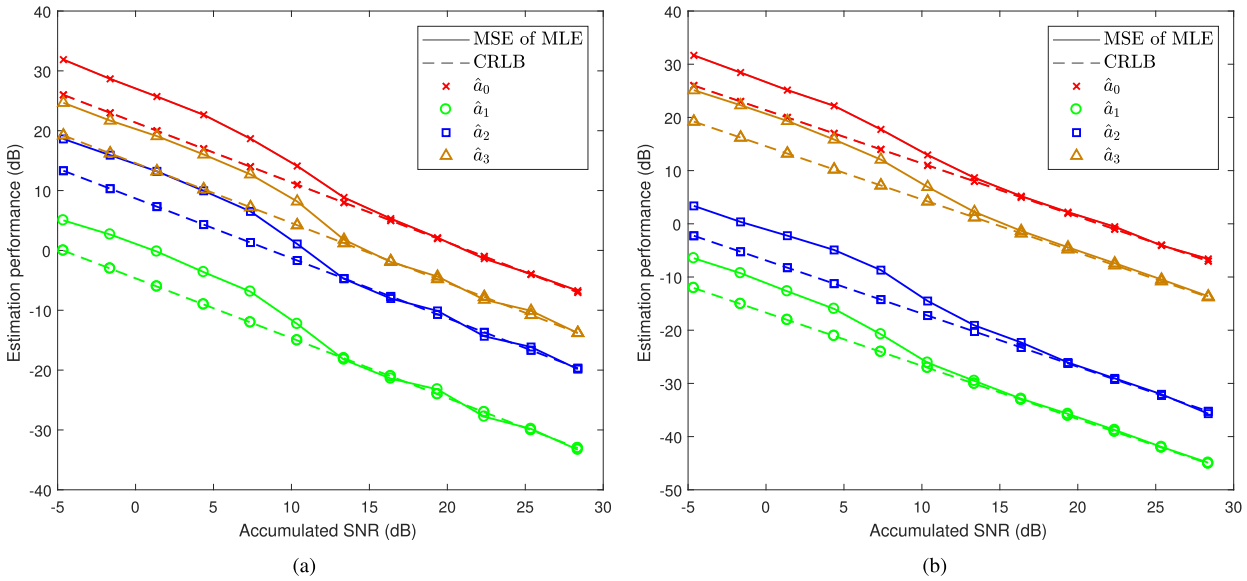

FIGURE 6. Comparisons of the MLE estimation performance and the CRLBs under a third-order motion model. (a) reference time factor $\eta = -\frac{1}{2}$. (b) reference time factor $\eta = 0$.

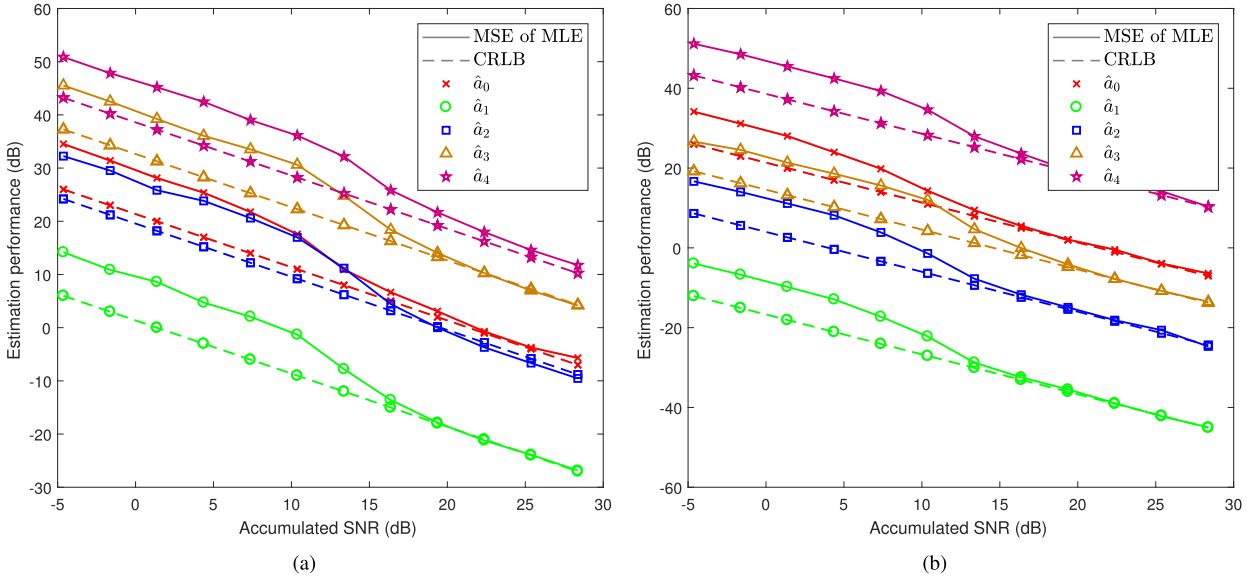

FIGURE 7. Comparisons of the MLE estimation performance and the CRLBs under a fourth-order motion model. (a) reference time factor $\eta = -\frac{1}{2}$. (b) reference time factor $\eta = 0$.

is better than that at $\eta = -\frac{1}{2}$, even over several orders of magnitude.

Third, we further investigate the comprehensive influences of the accumulated time T_D and the signal bandwidth B on the parameter estimation performance. In this simulation, the signal frequency is also set to 1 GHz and the accumulated SNR is 15 dB. A fourth order motion model ($I = 4$) is considered and the optional bandwidth $B = 5, 10, 50, 100$ MHz. T_D ranges from 0.1 s to 1.5 s with a step size of 0.2 s. The corresponding CRLB results versus T_D and B are illustrated in Fig. 3. It can be observed that the signal bandwidth B has a more significant impact on improving the range estimation performance. In contrast, the signal time length T_D has a more significant impact on improving the estimation performance of other high-order kinematic parameters. As mentioned before, due to the interference of the initial phase φ, the estimation performance of the radial range $\hat{a}_0$ is very different from that of other order kinematic parameters. This is also why the curve change trend of $\hat{a}_0$ is not as obvious in Fig. 1 and Fig. 2, although it is a polynomial function of η.

Finally, the MLE method is used to estimate the target's motion parameters at different SNR levels. It is

implemented with a "coarse" search followed by a "fine" search. We assume that the radar carrier frequency $f_c = 1$ GHz, the transmitting LFM waveform has a bandwidth $B = 5$ MHz, the coherent accumulated time $T_D = 1$ s, and the number of data points $M = K = 16$. Then, we have $N = 1089$. Four low-order motion models ($I = 1, 2, 3, 4$) are investigated separately. Under all the motion models, we choose $a_0 = 10$km, $a_1 = 100$m/s, $a_2 = 20$m/s^2, $a_3 = 15$m/s^3, and $a_4 = 8$m/s^4 as required. The signal amplitude and its initial phase $A = 1$ and $\varphi = \frac{\pi}{4}$. The accumulated SNR varies from -5 dB to 30 dB with a step size of 3 dB. The number of Monte Carlo simulations for each experiment is 500. Then, the average mean square error (MSE) of the MLE is calculated and compared with the corresponding CRLB, as illustrated from Fig. 4 to Fig. 7. It can be observed that the simulation results are quite consistent with the theoretical values for the kinematic parameters of all models and orders at high SNR. As the number of estimated parameters increases, a higher SNR threshold may be required.

VI. CONCLUSION

In this paper, Legendre polynomials and a linear mapping are effectively combined to derive the general CRLB expressions for jointly estimating the high-order kinematic parameters of maneuvering targets using an LFM coherent pulse train signal. And then, the CRLB performance relationships with relevant influencing factors, such as the motion model order, the reference time instant and the radar parameters, can be investigated analytically and quantitatively. The research shows that the derived CRLB results for the LFM pulse train signal differ from the pure PPS case in terms of the multiplicative factor and the initial phase. More importantly, it reveals the existing inconsistency of the optimal reference time instants for estimating the kinematic parameters of different models and orders. The reference time instant corresponding to the middle of the pulse train can be taken as a compromise choice, and in this situation, the CRLB of the same kinematic parameter experiences a stage change with the increasing of model order. As a result, the above exact and closed-form performance bounds can offer considerable potential in many applications.

We will conduct our future research from the following perspectives: The time-varying-amplitude case needs to be investigated due to the actual echo fluctuation of the target between pulses. The possible influences of other sampling schemes, such as nonuniform and random sampling, on the above CRLB results deserve in-depth and careful analysis. A more accurate echo signal model may be required, especially considering the Doppler shift and pulse spread effects caused by the target's high-speed motion. Moreover, this research can be further extended to other signal waveforms and some new application scenarios.

REFERENCES

[1] I. Djurović and M. Simeunović, "Review of the quasi maximum likelihood estimator for polynomial phase signals," *Digit. Signal Process.*, vol. 72, pp. 59–74, Jan. 2018.
[2] S. Peleg and B. Porat, "Estimation and classification of polynomial-phase signals," *IEEE Trans. Inf. Theory*, vol. 37, no. 2, pp. 422–430, Mar. 1991.
[3] B. Porat and B. Friedlander, "Asymptotic statistical analysis of the high-order ambiguity function for parameter estimation of polynomial-phase signals," *IEEE Trans. Inf. Theory*, vol. 42, no. 3, pp. 995–1001, May 1996.
[4] S. Barbarossa and V. Petrone, "Analysis of polynomial-phase signals by the integrated generalized ambiguity function," *IEEE Trans. Signal Process.*, vol. 45, no. 2, pp. 316–327, Feb. 1997.
[5] S. Barbarossa, A. Scaglione, and G. B. Giannakis, "Product high-order ambiguity function for multicomponent polynomial-phase signal modeling," *IEEE Trans. Signal Process.*, vol. 46, no. 3, pp. 691–708, Mar. 1998.
[6] L. Stanković, I. Djurović, S. Stanković, M. Simeunović, S. Djukanović, and M. Daković, "Instantaneous frequency in time–frequency analysis: Enhanced concepts and performance of estimation algorithms," *Digit. Signal Process.*, vol. 35, pp. 1–13, Dec. 2014.
[7] I. Djurović, M. Simeunović, and P. Wang, "Cubic phase function: A simple solution to polynomial phase signal analysis," *Signal Process.*, vol. 135, pp. 48–66, Jun. 2017.
[8] B. Barkat and B. Boashash, "Instantaneous frequency estimation of polynomial FM signals using the peak of the PWVD: Statistical performance in the presence of additive Gaussian noise," *IEEE Trans. Signal Process.*, vol. 47, no. 9, pp. 2480–2490, Sep. 1999.
[9] I. Djurović and M. Simeunović, "Combined HO-CF and HO-WD PPS estimator," *Signal, Image Video Process.*, vol. 9, no. 6, pp. 1395–1400, Sep. 2015.
[10] S. Shamsunder, G. B. Giannakis, and B. Friedlander, "Estimating random amplitude polynomial phase signals: A cyclostationary approach," *IEEE Trans. Signal Process.*, vol. 43, no. 2, pp. 492–505, Feb. 1995.
[11] G. Zhou, G. B. Giannakis, and A. Swami, "On polynomial phase signals with time-varying amplitudes," *IEEE Trans. Signal Process.*, vol. 44, no. 4, pp. 848–861, Apr. 1996.
[12] S. Peleg and B. Porat, "The Cramer-Rao lower bound for signals with constant amplitude and polynomial phase," *IEEE Trans. Signal Process.*, vol. 39, no. 3, pp. 749–752, Mar. 1991.
[13] B. Ristic and B. Boashash, "Comments on 'The Cramer-Rao lower bounds for signals with constant amplitude and polynomial phase,'" *IEEE Trans. Signal Process.*, vol. 46, no. 6, pp. 1708–1709, Jun. 1998.
[14] R. Rytel-Andrianik, "Exact Cramer-Rao bounds for signals with constant amplitude and polynomial phase," *Bull. Polish Acad. Sci., Tech. Sci.*, vol. 51, no. 3, pp. 421–433, 2003. [Online]. Available: https://yadda.icm.edu.pl/baztech/element/bwmeta1.element.baztech-article-BPG1-0010-0026
[15] J. A. Legg and D. A. Gray, "Performance bounds for polynomial phase parameter estimation with nonuniform and random sampling schemes," *IEEE Trans. Signal Process.*, vol. 48, no. 2, pp. 331–337, Feb. 2000.
[16] J. M. Francos and B. Friedlander, "Bounds for estimation of multicomponent signals with random amplitude and deterministic phase," *IEEE Trans. Signal Process.*, vol. 43, no. 5, pp. 1161–1172, May 1995.
[17] A. Swami, "Cramer-Rao bounds for deterministic signals in additive and multiplicative noise," *Signal Process.*, vol. 53, nos. 2–3, pp. 231–244, Sep. 1996.
[18] M. Ghogho, A. K. Nandi, and A. Swami, "Cramer-Rao bounds and maximum likelihood estimation for random amplitude phase-modulated signals," *IEEE Trans. Signal Process.*, vol. 47, no. 11, pp. 2905–2916, Nov. 1999.
[19] J. Xu, X.-G. Xia, S.-B. Peng, J. Yu, Y.-N. Peng, and L.-C. Qian, "Radar maneuvering target motion estimation based on generalized radon-Fourier transform," *IEEE Trans. Signal Process.*, vol. 60, no. 12, pp. 6190–6201, Dec. 2012.
[20] X. Li, G. Cui, W. Yi, and L. Kong, "A fast maneuvering target motion parameters estimation algorithm based on ACCF," *IEEE Signal Process. Lett.*, vol. 22, no. 3, pp. 270–274, Mar. 2015.
[21] L. Kong, X. Li, G. Cui, W. Yi, and Y. Yang, "Coherent integration algorithm for a maneuvering target with high-order range migration," *IEEE Trans. Signal Process.*, vol. 63, no. 17, pp. 4474–4486, Sep. 2015.
[22] P. Huang, G. Liao, Z. Yang, X.-G. Xia, J.-T. Ma, and J. Ma, "Long-time coherent integration for weak maneuvering target detection and high-order motion parameter estimation based on keystone transform," *IEEE Trans. Signal Process.*, vol. 64, no. 15, pp. 4013–4026, Aug. 2016.
[23] J. Zhang, T. Su, Y. Li, and J. Zheng, "Radar high-speed maneuvering target detection based on joint second-order keystone transform and modified integrated cubic phase function," *J. Appl. Remote Sens.*, vol. 10, no. 3, p. 035009, Aug. 2016.

[24] Y. Wang, J. Kang, and Y. Jiang, "ISAR imaging of maneuvering target based on the local polynomial Wigner distribution and integrated high-order ambiguity function for cubic phase signal model," *IEEE J. Sel. Topics Appl. Earth Observ. Remote Sens.*, vol. 7, no. 7, pp. 2971–2991, Jul. 2014.
[25] Y. Li, T. Su, and J. Zheng, "Inverse synthetic aperture radar imaging of targets with complex motions based on modified chirp rate–quadratic chirp rate distribution for cubic phase signal," *J. Appl. Remote Sens.*, vol. 9, no. 1, p. 095036, Dec. 2015.
[26] D. Li, X. Gui, H. Liu, J. Su, and H. Xiong, "An ISAR imaging algorithm for maneuvering targets with low SNR based on parameter estimation of multicomponent quadratic FM signals and nonuniform FFT," *IEEE J. Sel. Top. Appl. Earth Observ. Remote Sens.*, vol. 9, no. 12, pp. 5688–5702, Dec. 2016.
[27] T. J. Abatzoglou and G. O. Gheen, "Range, radial velocity, and acceleration MLE using radar LFM pulse train," *IEEE Trans. Aerosp. Electron. Syst.*, vol. 34, no. 4, pp. 1070–1083, Oct. 1998.
[28] Z. Deng, M. Fu, S. Jin, Y. Zhang, and Z. Wang, "Joint estimation of motion parameters using Newton's method," *IEEE Trans. Aerosp. Electron. Syst.*, vol. 51, no. 4, pp. 3386–3398, Oct. 2015.
[29] J. Xu, J. Yu, Y.-N. Peng, and X.-G. Xia, "Radon-Fourier transform for radar target detection, I: Generalized Doppler filter bank," *IEEE Trans. Aerosp. Electron. Syst.*, vol. 47, no. 2, pp. 1186–1202, Apr. 2011.
[30] X. Chen, J. Guan, N. Liu, and Y. He, "Maneuvering target detection via Radon-fractional Fourier transform-based long-time coherent integration," *IEEE Trans. Signal Process.*, vol. 62, no. 4, pp. 939–953, Feb. 2014.
[31] P.-P. Pan, H. Liu, Y.-X. Zhang, W. Qi, and Z.-M. Deng, "Range, radial velocity, and acceleration MLE using frequency modulation coded LFM pulse train," *Digit. Signal Process.*, vol. 60, pp. 252–261, Jan. 2017.
[32] S. Peleg, B. Porat, and B. Friedlander, "The achievable accuracy in estimating the instantaneous phase and frequency of a constant amplitude signal," *IEEE Trans. Signal Process.*, vol. 41, no. 6, pp. 2216–2224, Jun. 1993.
[33] R. McKilliam and A. Pollok, "On the Cramér–Rao bound for polynomial phase signals," *Signal Process.*, vol. 95, pp. 27–31, Feb. 2014.
[34] A. Pollok and R. McKilliam, "Modified Cramér–Rao bounds for continuous-phase modulated signals," *IEEE Trans. Commun.*, vol. 62, no. 5, pp. 1681–1690, May 2014.

SHUAI DING received the B.S. degree in electronic information science and technology from the College of Science, Xidian University, China, in 2010. He is currently pursuing the Ph.D. degree in information and communication engineering with the Beijing Institute of Technology, China. His research interests include radar system analysis, space debris surveillance, signal detection, and parameter estimation techniques.

DEFENG CHEN was born in Longyan, Fujian, China, in 1983. He received the B.S. and Ph.D. degrees in electronic engineering from the Beijing Institute of Technology, China, in 2006 and 2011, respectively. He is currently a Lecturer with the School of Information and Electronics, Beijing Institute of Technology. His research interests include radar signal processing and its applications in space target detection.

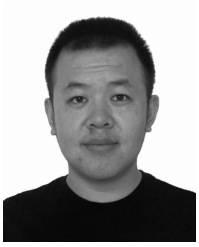

HUAWEI CAO received the B.S. degree in electronic science and technology from the Yanshan University, China, in 2009, and the Ph.D. degree in electronic engineering from the Beijing Institute of Technology, China, in 2016, respectively. He is currently a Post-Doctoral Researcher with the School of Information and Electronics, Beijing Institute of Technology. His research interests include radar system analysis and long-time coherent integration techniques for weak target detection.

TUO FU was born in Shenyang, Liaoning, China, in 1977. He received the Ph.D. degree in electronic engineering from the Beijing Institute of Technology, China, in 2004. From 2004 to 2006, he was a Post-Doctoral Researcher with the National Mobile Communications Research Laboratory, Southeast University, China. Since 2006, he has been an Associate Researcher with the School of Information and Electronics, Beijing Institute of Technology. His research interests include radar system design and statistical signal processing.